



A black carbon peak and its sources in the free troposphere of Beijing induced by cyclone lifting and transport from central China

Zhenbin Wang^{1,2,3,4}, Bin Zhu^{1,2,3,4}, Hanqing Kang^{1,2,3,4}, Wen Lu^{1,2,3,4}, Shuqi Yan^{1,2,3,4}, Delong Zhao⁵, Weihang Zhang⁶, and Jinhui Gao⁷

¹Collaborative Innovation Center on Forecast and Evaluation of Meteorological Disaster, Nanjing University of Information Science and Technology, Nanjing, 210044, China

²Key Laboratory for Aerosol-Cloud-Precipitation of China Meteorological Administration, Nanjing University of Information Science and Technology, Nanjing, 210044, China

³Key Laboratory of Meteorological Disaster (KLME), Ministry of Education, Nanjing University of Information Science and Technology, Nanjing, 210044, China

⁴Joint International Research Laboratory of Climate and Environment Change (ILCEC), Nanjing University of Information Science and Technology, Nanjing, 210044, China

⁵Beijing Weather Modification Office, Beijing, 100089, China

⁶College of Oceanic and Atmospheric Sciences, Ocean University of China, Qingdao, 266100, China

⁷Plateau Atmosphere and Environment Key Laboratory of Sichuan Province, School of Atmospheric Sciences, Chengdu University of Information Technology, Chengdu, 610225, China

Correspondence: Bin Zhu (binzhu@nuist.edu.cn)

Received: 21 April 2021 – Discussion started: 23 June 2021

Revised: 22 September 2021 – Accepted: 28 September 2021 – Published: 18 October 2021

Abstract. Observations suggest that the vertical distributions of air pollutants, such as black carbon (BC), present as various types depending on the emission sources and meteorological diffusion conditions. However, the formation process and source appointment of some special BC profiles are not fully understood. In this paper, by using the Weather Research and Forecasting model coupled with Chemistry (WRF-Chem) with a BC-tagging technique, we investigate the formation mechanism and regional sources of a BC peak in the free troposphere observed by an aircraft flight in Beijing (BJ) on 5 May 2018. The results show that the contribution rate of the Beijing–Tianjin–Hebei (BTH) region to the surface BC of BJ exceeded 80% in this case. Local sources dominated BC in BJ from the surface to approximately 700 m (78.5%), while the BC peak in the free troposphere (~4000 m) was almost entirely imported from external sources (99.8%). Combining BC tracking and process analysis, we find that horizontal advection (HADV) and vertical advection (VADV) processes played an important role in the convergent and upward movement and the transport of BC. The BC originating from the surface in

central provinces, including Shanxi (SX), Henan (HN), and Hebei (HB), had been uplifted through a cyclone system 16 h previously, was transported to a height of approximately 3000 m above BJ, and was then lifted by the VADV process to approximately 4000 m. At the surface, BJ and its surroundings were under the control of a weak pressure gradient, leading to the accumulation of BC within the boundary layer. Our results indicate that cyclone systems can quickly lift air pollutants, such as BC, up to the free troposphere, as well as extend their lifetimes and further affect the regional atmospheric environment and climate.

1 Introduction

Black carbon (BC) has been a research hotspot in recent years owing to its significant environmental and climate effects (IPCC, 2013). Unlike scattering aerosols (e.g. sulfate), BC has a strong ability to absorb solar radiation, which accelerates global warming (Jacobson, 2001; Weingartner et al., 2003; Bond et al., 2013). Additionally, BC can heat the upper

air of the planetary boundary layer (PBL), inhibit its development, and promote regional air pollution (Ding et al., 2016). Air quality is affected not only by local emissions but also by long-distance transport (Q. Zhang et al., 2017). For example, BC in south China is mainly transported from southeast Asia and north China (Fang et al., 2020), and most of the BC in the Arctic is transported from low-latitude regions (Keegan et al., 2014). Therefore, it is necessary to study the temporal and spatial distributions of BC and quantitatively analyse its regional sources to provide a reference for BC emission reduction.

The annual carbon emissions in China account for approximately one-quarter of the global carbon emissions (Bond et al., 2004). As the capital of China, Beijing (BJ) has experienced frequent air pollution in recent years (Van Pinxteren et al., 2009). In BJ and its surrounding areas, straw is often burned in early summer; hence, BC pollution has become an environmental problem that cannot be ignored (Bergin et al., 2001; He et al., 2001). However, most of the previous measurements of BC were performed at ground level, and the quantitative source tracking of BC was not thorough enough. For example, based on radiocarbon (^{14}C) measurements, Zhang et al. (2015) found that fossil emissions dominated BC with a mean contribution of $75 \pm 8\%$ in BJ, but regional source research was lacking. To identify the regional sources, Liu et al. (2018) used a potential source contribution function (PSCF) model to determine that Shanxi (SX) and Hebei (HB) were the main sources of BC in BJ but failed to quantify their separate contributions. Wen et al. (2020) used the Weather Research and Forecasting model coupled to chemistry (WRF-Chem) to simulate the regional contribution and found that regional transport contributes more than 40% to BC in BJ, but there was no detailed delineation of external source regions.

In addition to research on horizontal BC, many vertical observations have also been conducted in recent years, showing that vertical distributions of BC are strongly affected by meteorological conditions and regional transport. The aircraft observation experiment carried out in BJ showed that regional transport of BC can enhance air pollution and transport occurs not only near the surface but also in the middle levels of the PBL (0.5–1 km) (Zhao et al., 2015). Moreover, when the BC profile has a homogeneous or negative gradient distribution, the diurnal evolution of the PBL is the leading factor. When there is a positive BC gradient from the surface to the top of the PBL, it is mainly caused by surrounding emissions from high stacks and regional transport (Lu et al., 2019; Shi et al., 2021). However, these studies were mostly qualitative inferences, and it is difficult to quantify the formation process of vertical distributions and BC sources in detail. In addition, the effect of BC on the PBL varies greatly owing to its altitude. BC will inhibit the development of the PBL above the morning residual layer and conversely promote its development (Ma et al., 2020). Therefore, it is worth emphasizing that using only BC surface concentrations to calculate

radiative forcing and heating rates and ignoring the vertical distribution of BC will induce great uncertainties (Shi et al., 2021).

In summary, there are few studies on the quantitative interpretation of the regional contribution of BC or the source regions are not sufficiently separated; additionally, research on the reasons for and source tracking of the vertical distribution of BC is even scarcer. Based on the BC profile observed in BJ, this study uses the air quality model WRF-Chem with a BC-tagging technique to track the sources of BC, with the hope to explain the observed BC peak in the free troposphere and evaluate BC sources and direct BC regional emission reduction measures.

2 Data and methodology

2.1 Description of data used

2.1.1 Data used for modelling

A variety of data were used for modelling in this study. The initial and boundary meteorological and chemical conditions were provided by the National Centers for Environmental Prediction (NECP) final (FNL) operational global analysis data and outputs of the Community Atmosphere Model with Chemistry (CAM-chem; Lamarque et al., 2012). Anthropogenic emissions were provided by the Multi-resolution Emission Inventory for China (MEIC, 2016 version, <http://www.meicmodel.org/>, last access: 15 October 2021). Biogenic emissions were generated by using the Model of Emissions of Gases and Aerosols from Nature (MEGAN; Guenther et al., 2006).

2.1.2 Ground-based observation

In terms of the observation data used for model verification, the meteorological factors were derived from ground station observations using the Meteorological Information Comprehensive Analysis and Processing System (MICAPS) with a time accuracy of 3 h. $\text{PM}_{2.5}$ data were obtained from the China air quality online monitoring and analysis platform (<https://www.aqjstudy.cn/>, last access: 15 October 2021) provided by the Ministry of Ecology and Environment of China (<http://106.37.208.233:20035/>, last access: 15 October 2021), which includes 1500 monitoring stations. Each site was equipped with tapered element oscillating microbalance instruments (TEOM, RP1400 model, Thermo Scientific, USA) using the micro-oscillating balance method and the β -absorption method to measure $\text{PM}_{2.5}$ concentration at a resolution of $0.1 \mu\text{g m}^{-3}$ (Zhang and Cao, 2015). More details about the measurement methods, accuracy, and uncertainties are described in China's Environmental Protection Standard HJ 653-2013 (<http://www.cnemc.cn/jcgf/dqhj/201711/W020181008687887167307.pdf>, last access: 15 October 2021). Many studies on air pollution, par-

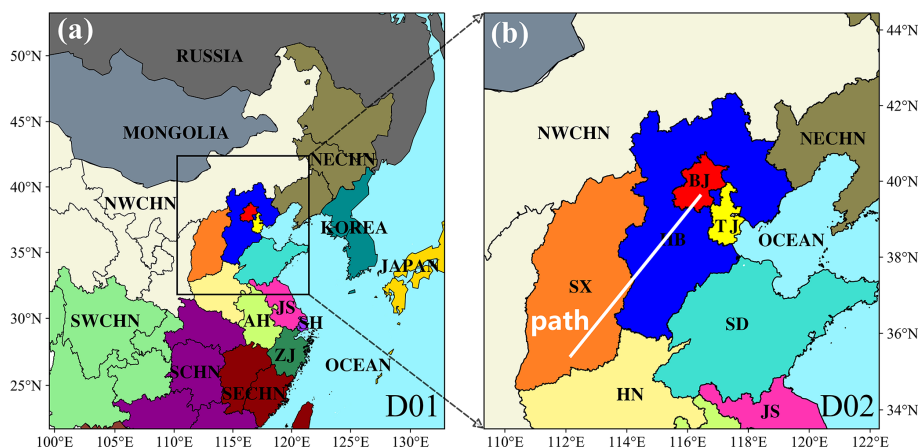


Figure 1. Model domain (the white line is the path of the vertical cross section in Sect. 3.3.2).

ticularly $\text{PM}_{2.5}$ pollution, have obtained their $\text{PM}_{2.5}$ data from this platform, such as Kang et al. (2021) and Hou et al. (2019, 2020). BC data were collected by the single-particle soot photometer (SP2, Droplet Measurement Technologies, Inc., USA) that was equipped with an external inlet, the Model 1200 passive isokinetic inlet (Brechtel Manufacturing Inc., USA), which could deliver a sample flow of 150 L min^{-1} with an air speed of 100 m s^{-1} and a sample efficiency of 95 % for particle sizes between 0.01 and $6 \mu\text{m}$. More details about SP2 can be found in Sharma et al. (2017) and Stephens et al. (2003).

2.1.3 Aircraft observation platform

In May 2018, we carried out a total of seven aircraft observations in BJ and surrounding areas (Fig. S1 in the Supplement), with each observation time between 10:00 and 12:00 BJT (Beijing time, also known as China standard time). The airborne measurements in this study were performed on a King Air 350 aircraft observation platform with a true speed of approximately $250\text{--}300 \text{ km h}^{-1}$. An Aircraft-Integrated Meteorological Measurement System (AIMMS-20, Aventech, Canada) was used to measure meteorological parameters in situ, including temperature (T), relative humidity (RH), wind speed (WS), and wind direction (WD), with a time resolution of 1 s. An SP2 was also installed on the aircraft observation platform to measure the vertical distribution of BC. The operation of most flights was carried out to avoid clouds where possible, which could effectively avoid the wet deposition of BC. More detailed information about the aircraft platform can be found in Tian et al. (2019), Hu et al. (2020), and Zhao et al. (2019, 2020).

2.2 Model description

The model used in this study, WRF-Chem 3.9.1.1, is coupled with a BC-tagging technique (Wang et al., 2014; Yang et al., 2017, 2018; Fang et al., 2020; Zhu et al., 2020), which is sim-

ilar to the particle source analysis technology in the Comprehensive Air Quality Model with Extensions (CAMx) model. The model can track the BC emitted from the predivided source region and quantitatively calculate the BC concentration in each source region one time. We divide the model domain into 20 geographic source regions before running the model, so the BC concentration of the target region is equal to the sum of the concentrations of BC from all source regions:

$$C = \sum_{i=1}^{20} C_i. \quad (1)$$

The model domain and the administrative regions of each source region are shown in Fig. 1 and Table 1, respectively (the source regions with less contribution will be merged in the subsequent analysis, defined as others). The BC concentration in each source region can be expressed as follows:

$$\Delta C_i = \Delta \text{Chem}_i + \Delta \text{Phy}_i + \Delta \text{Emis}_i, \quad (2)$$

where ΔChem_i , ΔPhy_i , and ΔEmis_i represent the BC concentration produced by chemical, physical and emission processes, respectively. However, BC is not included in the calculation of chemical reactions, so the value of ΔChem_i is 0. ΔPhy_i represents the concentration of BC changed by model physical processes, including horizontal advection, vertical advection, vertical mixing, dry deposition, wet deposition, and convection. The BC of each source region is regarded as an independent variable, and it is marked from the beginning of the BC emission, ΔEmis_i . The concentration of the total emissions in region i is defined as follows:

$$\Delta \text{Emis}_i(x, y, z) = \begin{cases} \Delta \text{Emis}_i(x, y, z) & \text{inside region } i \\ 0 & \text{outside region } i \end{cases}. \quad (3)$$

If BC is in region i , then $\Delta \text{Emis}_i(x, y, z) = \Delta \text{Emis}(x, y, z)$; otherwise, $\Delta \text{Emis}_i(x, y, z) = 0$. Subsequently, the newly defined variables will participate in the physical and chemical

calculation process in the model accompanied by the origin variables in the model. Thus, we can obtain the BC concentrations of each source region for any grid of the model and at any time.

Compared with sensitive experiments, this method can more accurately quantify the sources of BC with fewer errors. Previous studies have used a similar technique to study the source of air pollutants, such as $\text{PM}_{2.5}$ and O_3 , and the results all show that regional transport is an important factor of $\text{PM}_{2.5}$ and O_3 pollution in BJ (Gao et al., 2016, 2020; Y. Zhang et al., 2017). In addition, the air pollutants in BJ are mainly from BJ, TJ, and HB, and the high-concentration area presents a banded distribution feature from southwest to northeast, which is consistent with the analysis of BC in this study.

2.3 Parameterized scheme settings

Experiments started at 08:00 BJT on 1 May 2018 and ended at 08:00 BJT on 10 May 2018. The first 3 d was designated the spin-up time. Regarding the simulation settings, two nested domains (Fig. 1) were set up with grid sizes of 99×99 at horizontal resolutions of 36 and 12 km for D01 and D02, respectively. D01 covered most parts of China and the surrounding areas and ocean, and D02 covered most parts of north China. The modelling results of D01 provided meteorological and chemical boundary conditions for the simulations of D02. For the vertical direction, 38 layers were set up from the surface up to a pressure limit at 50 hPa, where 10 layers were located below 1 km. Notably, the carbon bond mechanism Z (CBM-Z; Zaveri and Peters, 1999) was applied as the gas-phase chemical mechanism in this study. Correspondingly, the Model for Simulating Aerosol Interactions and Chemistry with eight bins (MOSAIC-8bins; Zaveri et al., 2008) was chosen as the aerosol chemistry mechanism. Other parameterization settings are listed in Table 2.

3 Results and discussion

3.1 Model validation

Although the WRF-Chem model is widely used in air quality research, there are significant differences in the simulation results with different parameterization schemes. In this study, time series of both simulated and observed $\text{PM}_{2.5}$, BC concentration, temperature (T), and wind (Ua and Va) are shown in Fig. 2 to evaluate the performance of the model. Figure 2 illustrates that the model reproduces the numerical magnitude and variation characteristics of $\text{PM}_{2.5}$, BC, and meteorological factors well. Additionally, we calculate several common metrics – the correlation coefficient (r), index of agreement (IOA), mean bias (MB), root mean square error (RMSE), mean normalized bias (MNB), mean fractional bias (MFB), and total error (TE) – to validate the model performance for meteorological factors and air pollutants. The

benchmarks shown in brackets in Table 3 follow the recommended values suggested by Emery and Tai (2001) and US EPA (2007). Generally, the model reproduces the pollutants and main meteorological elements well, which provides a good basis for subsequent analysis. The model validation in north China, particularly in HN and SX (source regions), is presented in Figs. S2 and S3 and Tables S1 and S2 in the Supplement, and the modelling profiles of BC and meteorological factors are also presented in Fig. 6 in Sect. 3.2.2.

As shown in Table 3, meteorological factors (T , Ua , and Va) showed high values of the mean IOAs (≥ 0.75), indicating that the simulation agreed well with the observations. The MB of T was -0.25 , which suggested that the mean bias of T was within 1° , and the MBs of Ua and Va were -0.36 and -0.01 , respectively, suggesting that the model results deviated from the observations to a small extent. The RMSE and TE of meteorological elements were less than 1.88 and 1.44, respectively, which are comparable with the values reported in another modelling study (Gao et al., 2020) and were both within the threshold range. However, the MNB and MFB of Ua were beyond the scope of its benchmark, suggesting an overestimation of Ua . The MNB and MFB of the other meteorological factors were within the scope of their benchmark.

For air pollutants, good agreement was found between the simulations and observations since the IOAs of $\text{PM}_{2.5}$ and BC were 0.93 and 0.70, respectively. The MB values of BC and $\text{PM}_{2.5}$ were -0.42 and -11.2 , respectively, which demonstrated that the deviation in the MB between BC models and observations was less than $1 \mu\text{g m}^{-3}$, and the deviation in $\text{PM}_{2.5}$ was approximately $11 \mu\text{g m}^{-3}$. Notably, all the metrics of air pollutants also indicated that the model performance for air pollutants was acceptable.

3.2 Tracking BC from the surface to the free troposphere

During the aircraft observation on 5 May 2018, we found high BC values both near the ground and in the free troposphere (Fig. 3). To reveal the cause of the distinct BC profile, the WRF-Chem model with a BC-tagging technique was used for quantitative explanation.

3.2.1 Tracking BC sources at the surface

The near-surface pollution in BJ lasted from 5 to 6 May (Fig. 2), and both the spatial and temporal distributions (near-surface and in the free troposphere) of BC and $\text{PM}_{2.5}$ exhibited highly similar characteristics (Fig. S4). In the synoptic chart of Fig. 4a, there was a weak cyclone system in SX and NWCHN at 17:00 BJT on 4 May, leading to convergence and upward movement there. At 08:00 BJT on 5 May (Fig. 4b), the regions controlled by the weak cyclone system had expanded, including in SX, NWCHN, HB, and HN, while BJ was in front of the weak low pressure. At the same time,

Table 1. Source region division.

Source name	The administrative areas in each region
BJ	Beijing
TJ	Tianjin
HB	Hebei
SX	Shanxi
SD	Shandong
HN	Henan
AH	Anhui
JS	Jiangsu
NWCHN	Including Shaanxi, Gansu, Ningxia, Qinghai, Inner Mongolia, and Xiangjiang
MONGOLIA	Mongolia
NECHN	Including Heilongjiang, Liaoning, and Jilin
SWCHN	Including Yunnan, Guizhou, Sichuan, Chongqing, and Xizang
SECHN	Including Jiangxi, Fujian, and Taiwan
SCHN	Including Hunan, Hubei, Guangdong, and Guangxi
KOREA	Including North Korea and South Korea
JAPAN	Japan
RUSSIA	Russia
VIETNAM	Vietnam
ZJ	Zhejiang
SH	Shanghai
OCEAN	Including Bohai Sea, Yellow Sea, East China Sea, South China Sea, and western Pacific

Table 2. Major configuration options of WRF-Chem used for this study.

Item	Selection	Reference
PBL scheme	MYJ scheme	Janjic (2001)
Microphysics scheme	Lin scheme	Lin et al. (1983)
Long-wave radiation scheme	RRTM	Iacono et al. (2008)
Short-wave radiation scheme	RRTM	Iacono et al. (2008)
Land surface scheme	Noah land surface model	Chen and Dudhia (2001)
Dry-deposition scheme	Wesely scheme	Wesely (1989)

it can be seen that the near-surface convergence areas were mainly in SX from 4 to 5 May (Fig. 4d and e), corresponding to the position where the cyclone appeared, indicating that convergence uplift of surface BC existed in SX, which was consistent with the cross-section analysis in Sect. 3.3.2. There was convergence near the surface, and air pollutants in the surrounding areas were likely to accumulate, leading to an increase in BC concentration in BJ (Fig. 4d and e). Moreover, there was almost no convergence but an obvious “transport channel” from SX to BJ in the free troposphere (Fig. 4h), so BC was transported from SX to BJ by westerly winds. Subsequently, the low-pressure system moved south, and BJ was controlled by the uniform pressure field at 08:00 BJT on 6 May (Fig. 4c), which was not beneficial for the diffusion of BC in the horizontal and vertical directions (Fig. 4f). At an altitude of approximately 4000 m, BC was transported southward due to clean north winds (Fig. 4i).

Moreover, the sources of BC were quantitatively traced (Fig. 5) to explain the cause of pollution in BJ. The mean

BC concentration was $2.29 \mu\text{g m}^{-3}$ in this case (Fig. 5a), and the diurnal evolution of BC showed a characteristic of “lower in the daytime and higher in the nighttime”, which is related to the daily change in the PBL (Huang et al., 2018). Furthermore, BC near the surface mainly originated from BJ, HB, HN, TJ, and SD, whose mean contribution rates were 52.0 %, 23.9 %, 6.1 %, 5.7 %, and 4.4 %, respectively (Fig. 5b). The BC contribution rate of the BTH region to BJ exceeded 80 %, further confirming that when controlled by weak low pressure, air pollutants in surrounding areas are likely to accumulate in BJ and local pollutants have difficulty diffusing outward (Chen et al., 2008).

3.2.2 Tracking BC sources vertically

Near-surface BC mainly originated from BJ and its surrounding areas, while the source of BC in the free troposphere (~ 4000 m) showed different characteristics. The vertical distributions of BC and meteorological factors were

Table 3. Statistical indicators for evaluating the simulation results.

Variables	r	IOA	MB	RMSE	MNB	MFB	TE
T ($^{\circ}\text{C}$)	0.93	0.95 ([−0.5, 0.5])	−0.25 (≤ 2.0)	1.88 ([−0.15, 0.15])	−0.01 ([−0.6, 0.6])	−0.002 (≤ 2.0)	1.44
Ua (m s^{-1})	0.6	0.75	−0.36 ([−0.5, 0.5])	1.68 (≤ 2.0)	−2.32	2.01	1.26 (≤ 2.0)
Va (m s^{-1})	0.76	0.85	−0.01 ([−0.5, 0.5])	1.82 (≤ 2.0)	−0.02 ([−0.15, 0.15])	0.009 ([−0.6, 0.6])	1.41 (≤ 2.0)
BC ($\mu\text{g m}^{-3}$)	0.51	0.70	−0.42	1.47	−0.23	−0.06	1.02
PM _{2.5} ($\mu\text{g m}^{-3}$)	0.73	0.93	−11.2	33.79	−1.29	−0.06	26.48

Values that do not meet the threshold criteria are shown in bold.

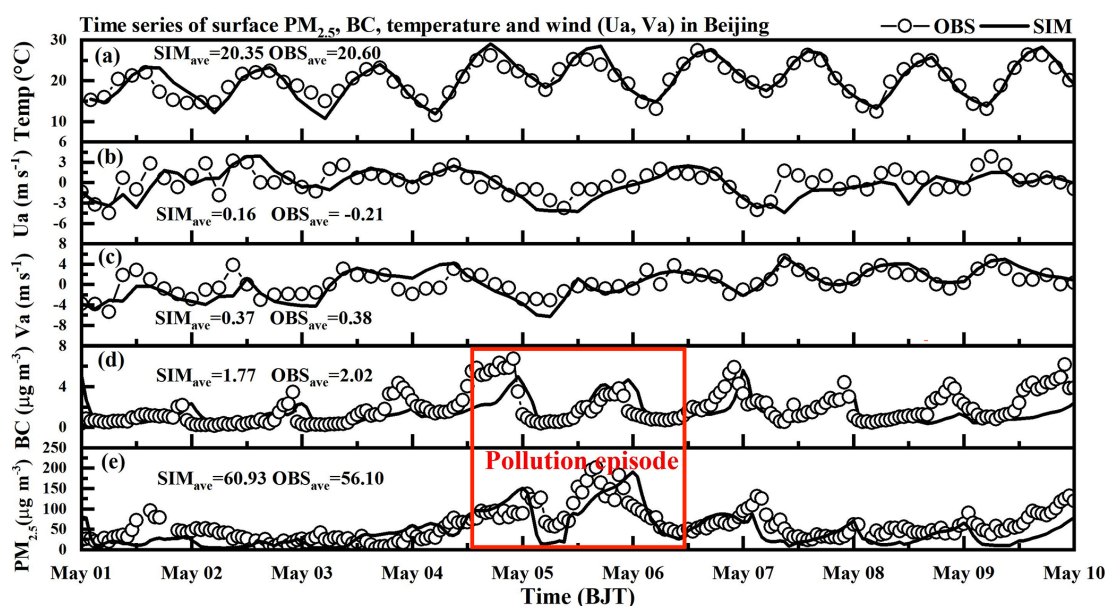


Figure 2. Time series of (a) temperature, (b) Ua , (c) Va , (d) BC, and (e) PM_{2.5} at Beijing station. The red box indicates the pollution episode in this study.

well simulated, especially BC, T , and RH (Fig. 6a and b). However, the WS under 2 km and WD at 1.25 km did not show agreements between SIM and OBS well, which could be attributed to local circulations such as land–sea and valley breezes across the complex terrain (Igel et al., 2018; Quan et al., 2020; Zhang et al., 2021). In this study, we focus more on the effect of upper-level winds on the transport of BC, and the winds at the altitude of 4000 m are significantly better modelled than the winds within the boundary layer. Overall, the model results are also acceptable in the vertical direction. The BC concentration presents a decreasing trend from the ground to approximately 700 m but increases from approximately 3000 m, forming a peak at an altitude of approximately 4000 m (Fig. 6a). As shown in Fig. 6e, the total contribution rate of BJ and HB below 700 m was as high

as 96.7%, which is related to the easterly wind near the surface (Fig. 6d). For the BC peak in the free troposphere (~ 4000 m), almost all BC was transported from external regions, including SX, NWCHN, SWCHN, HB, HN, and even SCHN, and the contribution rates were 24.7%, 23.5%, 10.5%, 9.4%, 8.9%, and 7.1%, respectively. In addition, Fig. 6d illustrates that this altitude was mainly controlled by westerly winds ($\sim 225^{\circ}$), and the wind speeds increased significantly above 3000 m, which is beneficial to the long-distance transport of BC.

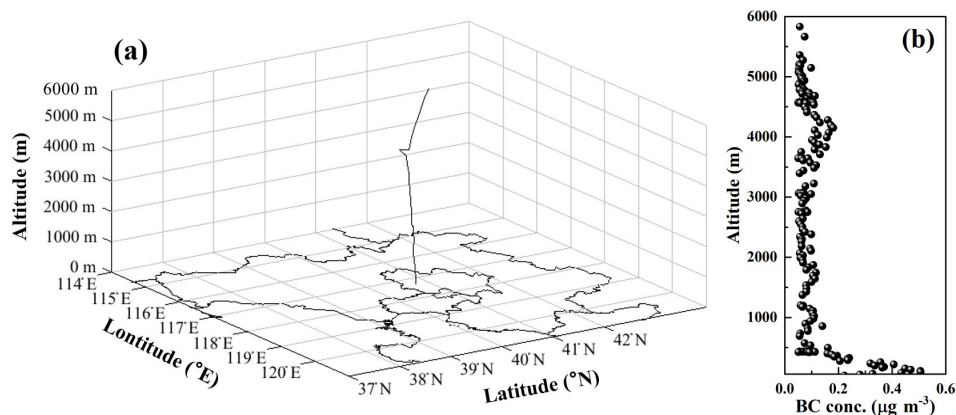


Figure 3. (a) Aircraft routes and (b) the BC profile observed at 10:00–11:00 BJT.

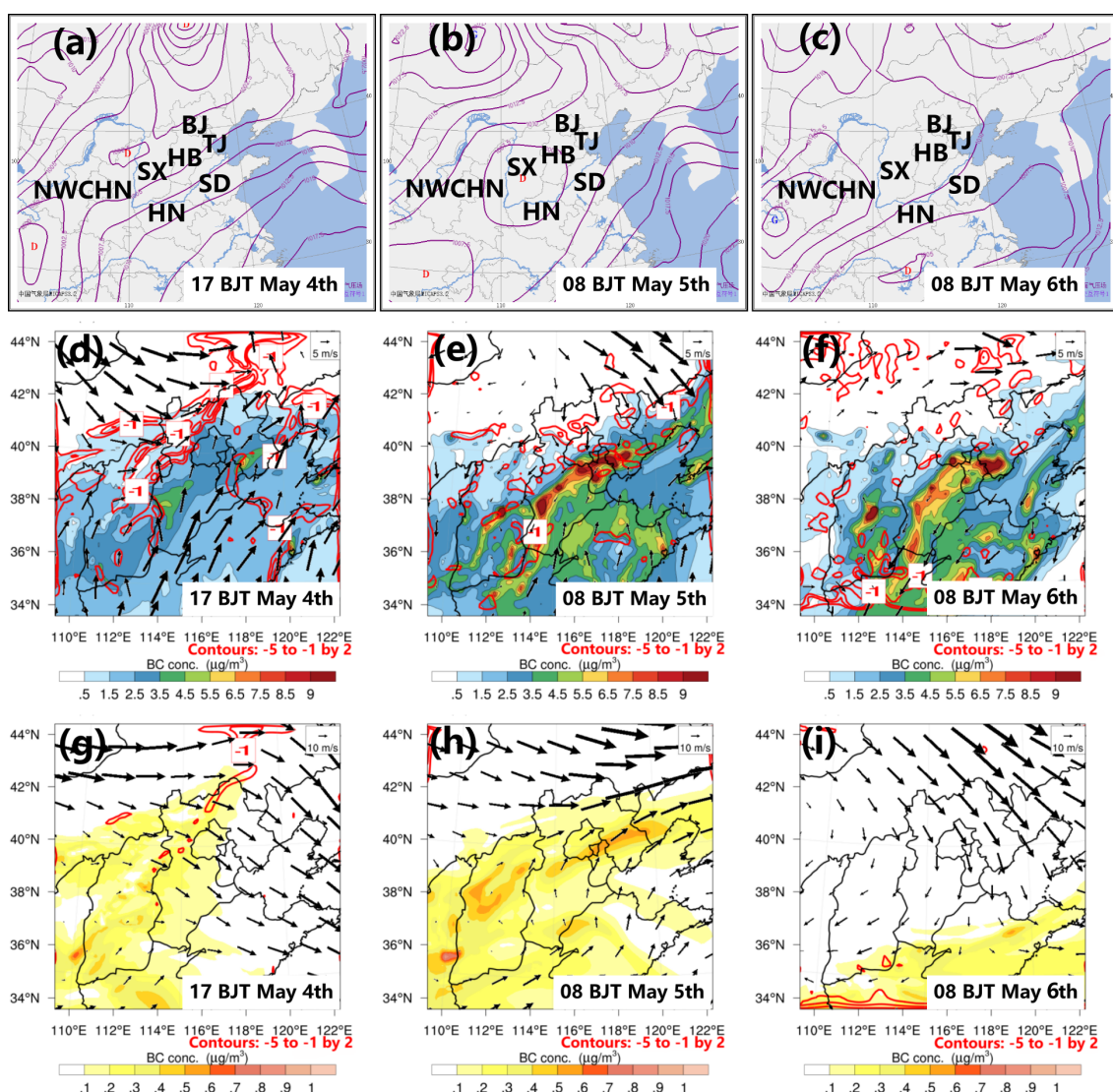


Figure 4. (a–c) Surface synoptic patterns, (d–f) BC concentration and wind vector at the surface, and (g–i) BC concentration and wind vector in the troposphere (~ 4000 m) at 17:00 BJT on 4 May, 08:00 BJT on 5 May, and 08:00 BJT on 6 May. The red line represents the convergence region (divergence < 0 ; unit $\times 10^{-6} \text{ s}^{-1}$).

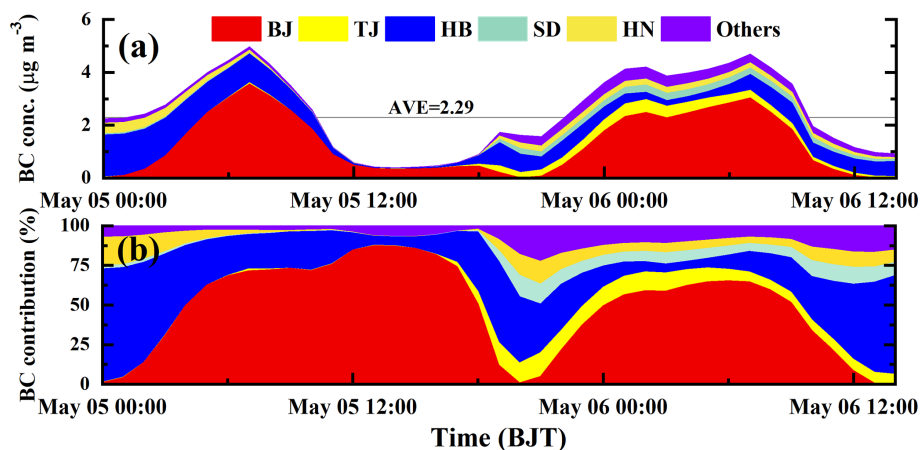


Figure 5. (a) BC concentration and (b) contribution rate of each source region to BC in BJ during the pollution episode. The legend refers to the regions shown in Fig. 1.

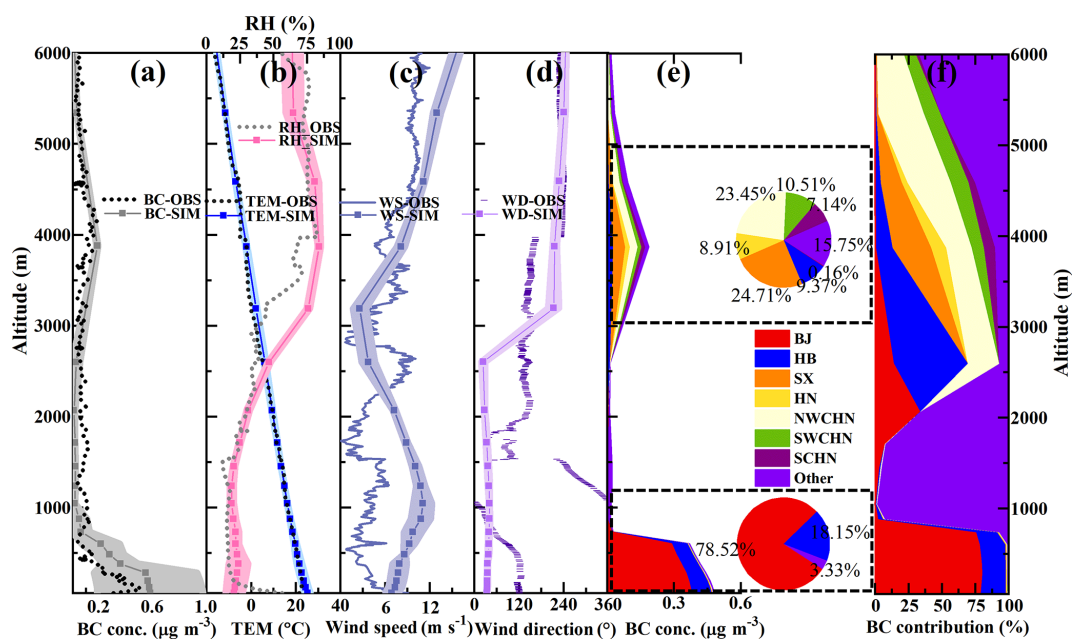


Figure 6. Model validation of (a) vertical BC, (b) T and RH, (c) WS, (d) WD, (e) BC concentration of each source region, and (f) contribution rate of each source region at 10:00–12:00 BJT on 5 May. The shading indicates the modelling standard deviation. The legend refers to the regions shown in Fig. 1.

3.3 Air mass trajectory and physical process analysis

3.3.1 Air mass trajectory analysis

To determine the source of BC in depth and to validate the source-tracing results above, we utilized the HYSPLIT model, developed by the National Oceanic and Atmospheric Administration (NOAA), to analyse the backward trajectory (24 h) of air masses reaching the altitudes of 600, 2200, and 3800 m above BJ, with intervals of 1600 m, at 08:00 BJT on 5 May (Fig. 7). As presented in Fig. 7, the air mass near the surface (red line) originated from BJ and its surround-

ing areas, which is consistent with the source-tracking results (Fig. 6e). The upper air mass (green line) originated in SX and reached BJ via HB, corresponding to the results of the cross section (Figs. 6e and 8). In addition, the air mass reaching the altitude of approximately 2000 m above BJ (blue line) was from Mongolia, a source region outside of D02, so the BC source-tracing results in a predominantly other source region (Fig. 6e, the other source region includes Mongolia and Inner Mongolia). Furthermore, the green line indicates that from 08:00 BJT on 4 May to 08:00 BJT on 5 May, there was an air mass rising from the surface in SX along a southwestern path and reaching the upper levels of BJ

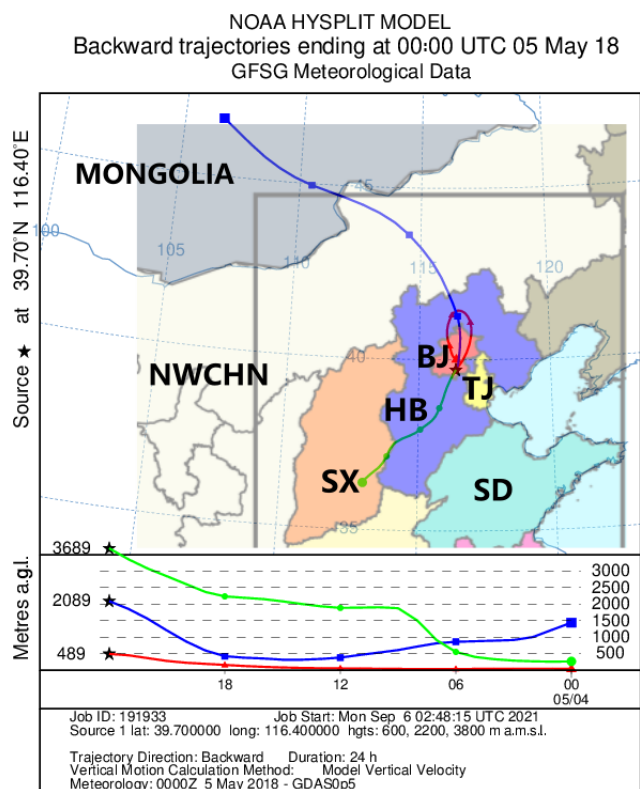


Figure 7. Backward trajectory (24 h) of the air mass at 08:00 BJT on 5 May.

(~ 4000 m). During this time, the conditions in central China (including SX, HB, and HN) were controlled by a cyclone system (Fig. 4a and b), leading to convergent and elevating motion there, which is conducive to the uplift of near-surface air masses and consistent with the backward trajectory model results.

3.3.2 Tracking BC sources in the cross section

In addition to the backward trajectory, the BC sources in the vertical cross section along the path from SX to BJ (in Figs. 1 and 7) can more convincingly explain the BC uplift and transport phenomenon. Referring to the backward trajectory, the white line shown in Fig. 1b can be regarded as the transport path of the air mass. To illustrate the uplift and transport mechanism of BC, cross sections of the BC concentration, wind vector, and BC contour lines (including BJ, SX, and NWCHN) along the aforementioned line are shown in Fig. 8. From 08:00 to 18:00 BJT on 4 May, the southwest wind prevailed along the SX–BJ line (Fig. 8a and b), which contributed to the transport of BC. BC originated in NWCHN, was transported to SX, and mixed with BC emitted in the SX region. By 16:00 BJT on 4 May, the ascending movement in SX was vigorous, resulting in the elevation of near-surface BC (Fig. 8b), which is consistent with the initial uplifting position presented in Fig. 7. BC originating

from NWCHN and SX was uplifted up to 3000 m and transported to HB and BJ to form high values (Fig. 8c). However, the wind direction near the surface changed from westerly to easterly, while westerly winds still prevailed in the upper air (Fig. 8d). As a result, near-surface BC in BJ diffused into the surrounding areas, such as HB, but in the upper air, BC originating in NWCHN and SX was still transported to BJ and lifted further to approximately 4000 m (Fig. 8d). At that point, there were high BC values both near the surface and in the free troposphere above BJ (~ 4000 m), which is consistent with the observation and source-tracing results in Fig. 6.

3.3.3 Physical process analysis

The backward trajectory shows that the air mass in the free troposphere originated from SX, while that within the boundary layer was from BJ; therefore, we further quantified the dominant transport processes of BC in the source region (SX) and receptor region (BJ), including horizontal advection (HADV), vertical advection (VADV), and vertical mixing (VMIX). In Fig. 9, the results show that HADV and VADV played an important role in the convergent and upward movement induced by cyclones and the transport of BC. From 14:00 BJT to approximately 18:00 BJT on 4 May, in the boundary layer (< 2 km), HADV made positive contributions to the BC concentration in SX, while the VADV had the opposite effect, suggesting that convergent and upward motion existed therein (Fig. 9a and b), which also corroborates the cyclone system in the surface synoptic patterns and near-surface convergence areas (Fig. 4a and d). At the same time, in the free troposphere (~ 4 km), the contribution of VADV and HADV to BC concentration was converse to that in the boundary layer, indicating that BC originating in SX was lifted from the surface to the free troposphere by VADV (Fig. 9a and b), which is consistent with the backward trajectory and cross-sectional analysis (Fig. 8b and c). In the upper layer of BJ (~ 3 km), HADV made a positive contribution to the BC concentration from 14:00 BJT to approximately 22:00 BJT on 4 May, showing that BC was transported from SX by westerly winds, which is also consistent with the analysis of BC transport in Fig. 4h. Then, VADV lifted the BC transported by the HADV to approximately 4 km from 02:00 BJT to approximately 08:00 BJT on 5 May (Fig. 9d and e), consistent with the analysis in Fig. 8c and d. VMIX in both SX and BJ occurred mainly in the afternoon of 4 May owing to intense turbulence (Fig. 9c and f).

4 Conclusions

This paper utilizes the air quality model WRF-Chem with a BC-tagging technique to study the formation mechanism of a special BC profile observed by an aircraft flight in BJ. The major findings are summarized as follows.

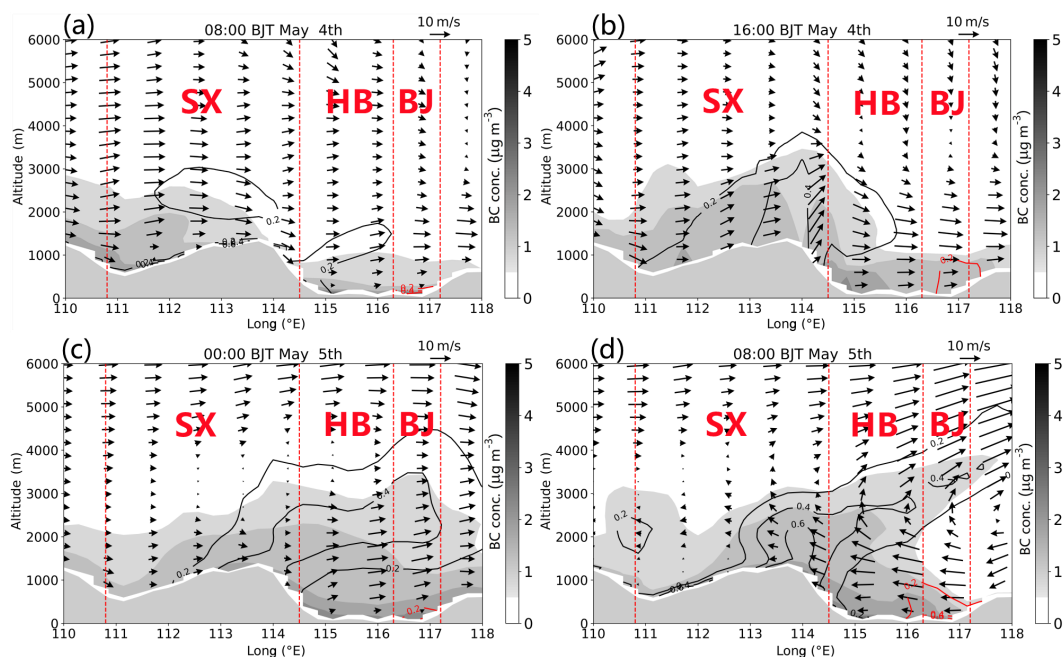


Figure 8. Vertical cross sections of BC concentration from SX to BJ and wind vectors (arrows) where the vertical speed is multiplied by 100 at (a) 08:00 BJT on 4 May, (b) 16:00 BJT on 4 May, (c) 00:00 BJT on 5 May, and (d) 08:00 BJT on 5 May. The black line is the BC contour lines of SX plus NWCHN, and the red line is the BC contour line of BJ.

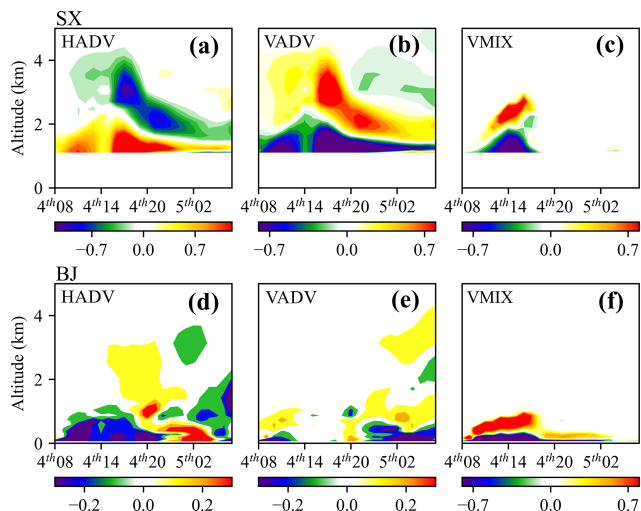


Figure 9. Contributions of horizontal advection (HADV), vertical advection (VADV), and vertical mixing (VMIX) processes to vertical BC concentrations in SX and BJ from 08:00 BJT on 4 May to 08:00 BJT on 5 May.

In this case, the mean BC concentration was $2.29 \mu\text{g m}^{-3}$. BC at the surface mainly originated from BJ, HB, HN, TJ, and SD, with contribution rates of 52.0%, 23.9%, 6.1%, 5.7% and 4.4%, respectively. The BC contribution rate of the BTH region to BJ exceeded 80%, further confirming that when controlled by weak low pressure, air pollutants in sur-

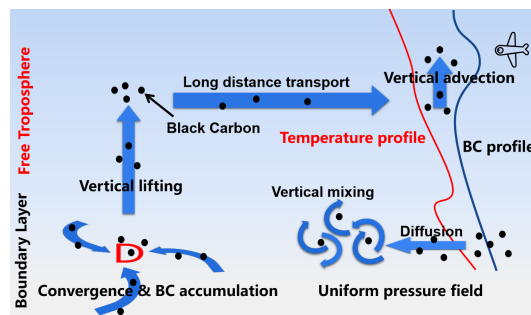


Figure 10. Formation mechanism of BC peak in the free troposphere.

rounding areas are likely to accumulate in BJ and local air pollutants have difficulty diffusing outward.

Local sources dominated BC in BJ from the surface to approximately 700 m (78.5%), while BC was almost entirely imported from external sources (99.8%) in the free troposphere (~ 4000 m). BC in the free troposphere mainly originated from SX, HB, HN, and NWCHN, and the contribution rates were 24.7%, 9.4%, 8.9%, and 23.5%, respectively.

Figure 10 illustrates the formation mechanism of the special BC profile. HADV and VADV processes played an important role in the convergent and upward movement and the transport of BC. Near-surface BC that originated from SX, HB, HN, and NWCHN had been uplifted by a cyclone system approximately 16 h previously, was transported to

a height of approximately 3000 m above BJ, and was then lifted by the VADV process to approximately 4000 m. At the surface, BJ and its surroundings were in the field of a weak pressure gradient, leading to the accumulation of BC.

The results indicate that cyclone systems can quickly lift air pollutants, such as BC, up to the free troposphere, extend their lifetimes, and further affect the regional atmospheric environment and climate.

Code and data availability. All the observations and model outputs mentioned in this study are publicly available. Observations of PM_{2.5} concentrations can be downloaded directly via the real-time release platform of the Ministry of Ecology and Environment of China (<https://quotsoft.net/air/>, last access: 15 October 2021) (Ministry of Ecology and Environment of China, 2021). Other observations and the simulated results can be accessed by contacting Zhenbin Wang at wangzb@nuist.edu.cn.

Supplement. The supplement related to this article is available online at: <https://doi.org/10.5194/acp-21-15555-2021-supplement>.

Author contributions. ZW performed the model simulation, data analysis, and manuscript writing. BZ proposed the idea, supervised this work, and revised the manuscript. DZ provided the observation data at BJ station. WL provided help with the model simulation. HK, SY, and WZ also contributed to the manuscript revision.

Competing interests. The contact author has declared that neither they nor their co-authors have any competing interests.

Disclaimer. Publisher's note: Copernicus Publications remains neutral with regard to jurisdictional claims in published maps and institutional affiliations.

Special issue statement. This article is part of the special issue "Satellite and ground-based remote sensing of aerosol optical, physical, and chemical properties over China". It is not associated with a conference.

Acknowledgements. We acknowledge the free use of MEIC emissions from Tsinghua University (<http://www.meicmodel.org/dataset-mix.html>, last access: 15 October 2021). We are grateful to the High Performance Computing Center of the Nanjing University of Information Science and Technology for performing the numerical calculations in this work on its blade cluster system.

Financial support. This work was supported by the National Key Research and Development Program (grant no. 2016YFA0602003)

and National Natural Science Foundation of China (grant nos. 42021004 and 92044302).

Review statement. This paper was edited by Stelios Kazadzis and reviewed by two anonymous referees.

References

- Bergin, M. H., Cass, G. R., Xu, J., Fang, C., Zeng, L. M., Yu, T., Salmon, L. G., Kiang, C. S., Tang, X. Y., Zhang, Y. H., and Chameides, W. L.: Aerosol radiative, physical, and chemical properties in Beijing during June 1999, *J. Geophys. Res.-Atmos.*, 106, 17969–17980, <https://doi.org/10.1029/2001JD900073>, 2001.
- Bond, T. C., Streets, D. G., Yarber, K. F., Nelson, S. M., Woo, J. H., and Klimont, Z.: A technology-based global inventory of black and organic carbon emissions from combustion, *J. Geophys. Res.-Atmos.*, 109, D14203, <https://doi.org/10.1029/2003JD003697>, 2004.
- Bond, T. C., Doherty, S. J., Fahey, D. W., Forster, P. M., Berntsen, T., DeAngelo, B. J., Flanner, M. G., Ghan, S., Kärcher, B., Koch, D., Kinne, S., Kondo, Y., Quinn, P. K., Sarofim, M. C., Schultz, M. G., Schulz, M., Venkataraman, C., Zhang, H., Zhang, S., Bellouin, N., Guttikunda, S. K., Hopke, P. K., Jacobson, M. Z., Kaiser, J. W., Klimont, Z., Lohmann, U., Schwarz, J. P., Shindell, D., Storelvmo, T., Warren, S. G., and Zender, C. S.: Bounding the role of black carbon in the climate system: a scientific assessment, *J. Geophys. Res.-Atmos.*, 118, 5380–5552, <https://doi.org/10.1002/jgrd.50171>, 2013.
- Chen, F. and Dudhia, J.: Coupling an advanced land surface–hydrology model with the Penn state–NCAR MM5 modeling system. part I: model implementation and sensitivity, *Mon. Weather Rev.*, 129, 569–585, [https://doi.org/10.1175/1520-0493\(2001\)129<0569:CAALSH>2.0.CO;2](https://doi.org/10.1175/1520-0493(2001)129<0569:CAALSH>2.0.CO;2), 2001.
- Chen, Z. H., Cheng, S. Y., Li, J. B., Guo, X. R., Wang, W. H., and Chen, D. S.: Relationship between atmospheric pollution processes and synoptic pressure patterns in northern China, *Atmos. Environ.*, 42, 6078–6087, <https://doi.org/10.1016/j.atmosenv.2008.03.043>, 2008.
- Ding, A. J., Huang, X., Nie, W., Sun, J. N., Kerminen, V. M., Petäjä, T., Su, H., Cheng, Y. F., Yang, X. Q., Wang, M. H., Chi, X. G., Wang, J. P., Virkkula, A., Guo, W. D., Yuan, J., Wang, S. Y., Zhang, R. J., Wu, Y. F., Song, Y., Zhu, T., Zilitinkevich, S., Kulmala, M., and Fu, C. B.: Enhanced haze pollution by black carbon in megacities in China, *Geophys. Res. Lett.*, 43, 2873–2879, <https://doi.org/10.1002/2016GL067745>, 2016.
- Emery, C. and Tai, E.: Enhanced Meteorological Modeling and Performance Evaluation for Two Texas Ozone Episodes, Final Report Submitted to Texas Natural Resources Conservation Commission, ENVIRON, International Corporation, Novato, USA, 2001.
- Fang, C., Zhu, B., Pan, C., Yun, X., Ding, D., and Tao, S.: Regional and sectoral sources for black carbon over South China in spring and their sensitivity to east Asian summer monsoon onset, *J. Geophys. Res.-Atmos.*, 125, e2020JD033219, <https://doi.org/10.1029/2020JD033219>, 2020.

- Gao, J., Zhu, B., Xiao, H., Kang, H., Hou, X., and Shao, P.: A case study of surface ozone source apportionment during a high concentration episode, under frequent shifting wind conditions over the Yangtze River Delta, China, *Sci. Total Environ.*, 544, 853–863, <https://doi.org/10.1016/j.scitotenv.2015.12.039>, 2016.
- Gao, J., Li, Y., Zhu, B., Hu, B., Wang, L., and Bao, F.: What have we missed when studying the impact of aerosols on surface ozone via changing photolysis rates?, *Atmos. Chem. Phys.*, 20, 10831–10844, <https://doi.org/10.5194/acp-20-10831-2020>, 2020.
- Guenther, A., Karl, T., Harley, P., Wiedinmyer, C., Palmer, P. I., and Geron, C.: Estimates of global terrestrial isoprene emissions using MEGAN (Model of Emissions of Gases and Aerosols from Nature), *Atmos. Chem. Phys.*, 6, 3181–3210, <https://doi.org/10.5194/acp-6-3181-2006>, 2006.
- He, K., Yang, F., Ma, Y., Zhang, Q., Yao, X., Chan, C. K., Cadle, S., Chan, T., and Mulawa, P.: The characteristics of PM_{2.5} in Beijing, China, *Atmos. Environ.*, 35, 4959–4970, [https://doi.org/10.1016/S1352-2310\(01\)00301-6](https://doi.org/10.1016/S1352-2310(01)00301-6), 2001.
- Hou, X., Zhu, B., Kumar, K. R., and Lu, W.: Inter-annual variability in fine particulate matter pollution over China during 2013–2018: Role of meteorology, *Atmos. Environ.*, 214, 116842, <https://doi.org/10.1016/j.atmosenv.2019.116842>, 2019.
- Hou, X., Zhu, B., Kumar, K. R., de Leeuw, G., Lu, W., Huang, Q., and Zhu, X.: Establishment of conceptual schemas of surface synoptic meteorological situations affecting fine particulate pollution across eastern China in the winter, *J. Geophys. Res.*, 125, e2020JD033153, <https://doi.org/10.1029/2020JD033153>, 2020.
- Hu, K., Zhao, D., Liu, D., Ding, S., Tian, P., Yu, C., Zhou, W., Huang, M., and Ding, D.: Estimating radiative impacts of black carbon associated with mixing state in the lower atmosphere over the northern North China Plain, *Chemosphere*, 252, 126455, <https://doi.org/10.1016/j.chemosphere.2020.126455>, 2020.
- Huang, X., Wang, Z., and Ding, A.: Impact of aerosol-PBL interaction on haze pollution: multiyear observational evidences in North China, *Geophys. Res. Lett.*, 45, 8596–8603, <https://doi.org/10.1029/2018GL079239>, 2018.
- Iacono, M. J., Delamere, J. S., Mlawer, E. J., Shephard, M. W., Clough, S. A., and Collins, W. D.: Radiative forcing by long-lived greenhouse gases: calculations with the AER radiative transfer models, *J. Geophys. Res.-Atmos.*, 113, D13103, <https://doi.org/10.1029/2008JD009944>, 2008.
- Igel, A. L., van den Heever, S. C., and Johnson, J. S.: Meteorological and land surface properties impacting sea breeze extent and aerosol distribution in a dry environment, *J. Geophys. Res.-Atmos.*, 123, 22–37, <https://doi.org/10.1002/2017JD027339>, 2018.
- IPCC: Contribution of Working Group I to the Fifth Assessment Report of the Intergovernmental Panel on Climate Change, Cambridge University Press, Cambridge, UK and New York, USA, 2013.
- Jacobson, M. Z.: Strong radiative heating due to the mixing state of black carbon in atmospheric aerosols, *Nature*, 409, 695–697, <https://doi.org/10.1038/35055518>, 2001.
- Janjic, Z. I.: Nonsingular Implementation of the Mellor-Yamada Level 2.5 Scheme in the NCEP Meso Model, NCEP Technical Note 437, p. 61, available at: <https://repository.library.noaa.gov/view/noaa/11409> (last access: 15 October 2021), 2001.
- Kang, H., Zhu, B., Liu, X., Shi, S., Hou, X., Lu, W., Yan, S., Pan, C., and Chen, Y.: Three-dimensional distribution of PM_{2.5} over the yangtze river delta as cold fronts moving through, *J. Geophys. Res.*, 126, e2020JD034035, <https://doi.org/10.1029/2020JD034035>, 2021.
- Keegan, K. M., Albert, M. R., McConnell, J. R., and Baker, I.: Climate change and forest fires synergistically drive widespread melt events of the Greenland Ice Sheet, *P. Natl. Acad. Sci. USA*, 111, 7964–7967, <https://doi.org/10.1073/pnas.1405397111>, 2014.
- Lamarque, J. F., Emmons, L., Hess, P., Kinnison, D. E., Tilmes, S., Vitt, F., Heald, C., Holland, E. A., Lauritzen, P., and Neu, J.: CAM-chem: description and evaluation of interactive atmospheric chemistry in the community earth system model, *Geosci. Model Dev.*, 5, 369–411, <https://doi.org/10.5194/gmd-5-369-2012>, 2012.
- Lin, Y. L., Farley, R. D., and Orville, H. D.: Bulk parameterization of the snow field in a cloud model, *J. Appl. Meteorol. Clim.*, 22, 1065–1092, [https://doi.org/10.1175/1520-0450\(1983\)022<1065:BPOTSF>2.0.CO;2](https://doi.org/10.1175/1520-0450(1983)022<1065:BPOTSF>2.0.CO;2), 1983.
- Liu, Y., Yan, C., and Zheng, M.: Source apportionment of black carbon during winter in Beijing, *Sci. Total Environ.*, 618, 531–541, <https://doi.org/10.1016/j.scitotenv.2017.11.053>, 2018.
- Lu, Y., Zhu, B., Huang, Y., Shi, S., Wang, H., An, J., and Yu, X.: Vertical distributions of black carbon aerosols over rural areas of the Yangtze River Delta in winter, *Sci. Total Environ.*, 661, 1–9, <https://doi.org/10.1016/j.scitotenv.2019.01.170>, 2019.
- Ma, Y., Ye, J., Xin, J., Zhang, W., Vilà-Guerau de Arellano, J., Wang, S., Zhao, D., Dai, L., Ma, Y., and Wu, X.: The stove, dome, and umbrella effects of atmospheric aerosol on the development of the planetary boundary layer in hazy regions, *Geophys. Res. Lett.*, 47, e2020GL087373, <https://doi.org/10.1029/2020GL087373>, 2020.
- Ministry of Ecology and Environment of China: <https://quotsoft.net/air/>, last access: 15 October 2021.
- Quan, J., Dou, Y., Zhao, X., Liu, Q., Sun, Z., Pan, Y., Jia, X., Cheng, Z., Ma, P., Su, J., and Xin, J.: Regional atmospheric pollutant transport mechanisms over the North China Plain driven by topography and planetary boundary layer processes, *Atmos. Environ.*, 221, 117098, <https://doi.org/10.1016/j.atmosenv.2019.117098>, 2020.
- Sharma, S., Leitch, W. R., Huang, L., Weber, D., Kolonjari, F., Zhang, W., Hanna, S. J., Bertram, A. K., and Ogren, J. A.: An evaluation of three methods for measuring black carbon in Alert, Canada, *Atmos. Chem. Phys.*, 17, 15225–15243, <https://doi.org/10.5194/acp-17-15225-2017>, 2017.
- Shi, S., Zhu, B., Lu, W., Yan, S., Fang, C., Liu, X., Liu, D., and Liu, C.: Estimation of radiative forcing and heating rate based on vertical observation of black carbon in Nanjing, China, *Sci. Total Environ.*, 756, 135–144, <https://doi.org/10.1016/j.scitotenv.2020.144135>, 2021.
- Stephens, M., Turner, N., and Sandberg, J.: Particle identification by laser-induced incandescence in a solid-state laser cavity, *Appl. Optics*, 42, 3726–3736, <https://doi.org/10.1364/AO.42.003726>, 2003.
- Tian, P., Liu, D., Huang, M., Liu, Q., Zhao, D., Ran, L., Deng, Z., Wu, Y., Fu, S., Bi, K., Gao, Q., He, H., Xue, H., and Ding, D.: The evolution of an aerosol event observed from aircraft in Beijing: an insight into regional pollution transport, *Atmos. Environ.*, 206, 11–20, <https://doi.org/10.1016/j.atmosenv.2019.02.005>, 2019.

- US EPA: Guidance on the Use of Models and Other Analyses for Demonstrating Attainment of Air Quality Goals for Ozone, PM_{2.5}, and Regional Haze, EPA-454/B-07-002, available at: <https://nepis.epa.gov/Exe/ZyPURL.cgi?Dockey=P1006FPU.TXT> (last access: 15 October 2021), 2007.
- Van Pinxteren, D., Brüggemann, E., Gnauk, T., Iinuma, Y., Müller, K., Nowak, A., Achtert, P., Wiedensohler, A., and Herrmann, H.: Size- and time-resolved chemical particle characterization during CAREBeijing-2006: different pollution regimes and diurnal profiles, *J. Geophys. Res.-Atmos.*, 114, D00G09, <https://doi.org/10.1029/2008JD010890>, 2009.
- Wang, H., Rasch, P. J., Easter, R. C., Singh, B., Zhang, R., Ma, P. L., Qian, Y., Ghan, S. J., and Beagley, N.: Using an explicit emission tagging method in global modeling of source-receptor relationships for black carbon in the Arctic: Variations, sources, and transport pathways, *J. Geophys. Res.-Atmos.*, 119, 12888–12909, <https://doi.org/10.1002/2014JD022297>, 2014.
- Weingartner, E., Saathoff, H., Schnaiter, M., Streit, N., Bitnar, B., and Baltensperger, U.: Absorption of light by soot particles: determination of the absorption coefficient by means of aethalometers, *J. Aerosol Sci.*, 34, 1445–1463, [https://doi.org/10.1016/S0021-8502\(03\)00359-8](https://doi.org/10.1016/S0021-8502(03)00359-8), 2003.
- Wen, W., Ma, X., Guo, C., Wei, P., Zhao, X., and Xu, J.: Source apportionment of black carbon and the feedback effect on the meteorological factors in Beijing, China, *Environ. Sci. Pollut. Res.*, 27, 41764–41775, <https://doi.org/10.1007/s11356-020-09881-z>, 2020.
- Wesely, M. L.: Parameterization of surface resistances to gaseous dry deposition in regional-scale numerical-models, *Atmos. Environ.*, 23, 1293–1304, <https://doi.org/10.1016/j.atmosenv.2007.10.058>, 1989.
- Yang, Y., Wang, H., Smith, S. J., Ma, P. L., and Rasch, P. J.: Source attribution of black carbon and its direct radiative forcing in China, *Atmos. Chem. Phys.*, 17, 4319–4336, <https://doi.org/10.5194/acp-17-4319-2017>, 2017.
- Yang, Y., Wang, H., Smith, S. J., Zhang, R., Lou, S., Yu, H., Li, C., and Rasch, P. J.: Source apportionments of aerosols and their direct radiative forcing and long-term trends over continental United States, *Earth's Future*, 6, 793–808, <https://doi.org/10.1029/2018EF000859>, 2018.
- Zaveri, R. A. and Peters, L. K.: A new lumped structure photochemical mechanism for large-scale applications, *J. Geophys. Res.-Atmos.*, 104, 30387–30415, <https://doi.org/10.1029/1999JD900876>, 1999.
- Zaveri, R. A., Easter, R. C., Fast, J. D., and Peters, L. K.: Model for simulating aerosol interactions and chemistry (MOSAIC), *J. Geophys. Res.-Atmos.*, 113, D13204, <https://doi.org/10.1029/2007JD008782>, 2008.
- Zhang, Q., Jiang, X., Tong, D., Davis, S. J., Zhao, H., Geng, G., Feng, T., Zheng, B., Lu, Z., and Streets, D. G.: Transboundary health impacts of transported global air pollution and international trade, *Nature*, 543, 705–709, <https://doi.org/10.1029/2007JD008782>, 2017.
- Zhang, W. H., Hai, S., Zhao, Y., Sheng, L., Zhou, Y., Wang, W., and Li, W.: Numerical modeling of regional transport of PM_{2.5} during a severe pollution event in the Beijing–Tianjin–Hebei region in November 2015, *Atmos. Environ.*, 254, 118393, <https://doi.org/10.1016/j.atmosenv.2021.118393>, 2021.
- Zhang, Y., Zhu, B., Gao, J., Kang, H., Yang, P., Wang, L., and Zhang, J.: The source apportionment of primary PM_{2.5} in an aerosol pollution event over Beijing–Tianjin–Hebei region using WRF-Chem, *China, Aerosol Air Qual. Res.*, 17, 2966–2980, <https://doi.org/10.4209/aaqr.2016.10.0442>, 2017.
- Zhang, Y. L. and Cao, F.: Fine particulate matter (PM_{2.5}) in China at a city level, *Sci. Rep.* 5, 14884, <https://doi.org/10.1038/srep14884>, 2015.
- Zhang, Y. L., Huang, R. J., El Haddad, I., Ho, K. F., Cao, J. J., Han, Y., Zotter, P., Bozzetti, C., Daellenbach, K. R., and Canonaco, F.: Fossil vs. non-fossil sources of fine carbonaceous aerosols in four Chinese cities during the extreme winter haze episode of 2013, *Atmos. Chem. Phys.*, 15, 1299–1312, <https://doi.org/10.5194/acp-15-1299-2015>, 2015.
- Zhao, D., Tie, X., Gao, Y., Zhang, Q., Tian, H., Bi, K., Jin, Y., and Chen, P.: In-situ aircraft measurements of the vertical distribution of black carbon in the lower troposphere of Beijing, China, in the spring and summer time, *Atmosphere*, 6, 713–731, <https://doi.org/10.3390/atmos6050713>, 2015.
- Zhao, D., Huang, M., Tian, P., He, H., Lowe, D., Zhou, W., Sheng, J., Wang, F., Bi, K., Kong, S., Yang, Y., Liu, Q., Liu, D., and Ding, D.: Vertical characteristics of black carbon physical properties over Beijing region in warm and cold seasons, *Atmos. Environ.*, 213, 296–310, <https://doi.org/10.1016/j.atmosenv.2019.06.007>, 2019.
- Zhao, D., Liu, D., Yu, C., Tian, P., Hu, D., Zhou, W., Ding, S., Hu, K., Sun, Z., Huang, M., Huang, Y., Yang, Y., Wang, F., Shen, J., Liu, Q., Kong, S., Li, X., He, H., and Ding, D.: Vertical evolution of black carbon characteristics and heating rate during a haze event in Beijing winter, *Sci. Total Environ.*, 709, 136–251, 2020.
- Zhu, B., Wang, Y. M., Gao, J. H., Zhao, T. L., and Wang, L. R.: Distribution and source characteristics of Black carbon in autumn over Hunan-Hubei basin, China, *Trans. Atmos. Sci.*, 43, 592–602, <https://doi.org/10.13878/j.cnki.dqkxxb.20200422001>, 2020.